MORPHOLOGY OF IMPACT CRATERS GENERATED BY HYPERVELOCITY MICRON-SIZED OLIVINE AND IRON PARTICLES

Y. W. Li[(1)], R. Srama[(1)], S. Bugiel[(1)], A. Schilling[(1)], M. Trieloff[(2)], Jon K. Hillier[(2)], F. Postberg[(2)], K. Fiege[(2)], Y. Y. Wu[(3)], and E. Grün[(4)]

[(1)]*IRS, University of Stuttgart, 70569 Stuttgart, Germany, Email: {li, srama}@irs.uni-stuttgart.de*
[(2)]*Institut für Geowissenschaften, Universität Heidelberg, 69120 Heidelberg, Germany*
[(3)]*Harbin Institute of Technology, 150001 Harbin, China*
[(4)]*LASP, University of Colorado, Boulder, Colorado 80309, USA*

ABSTRACT

In order to understand the process of cosmic dust particle impacts and translate crater shape on smoothed metallic surfaces to dust properties, correct calibration of the experimental impact data is needed. This article presents the results of studies of crater morphology generated by impact using new mineral (olivine) particles. The goal of our study was to characterize the similarities and differences of impact craters created by olivine and iron particles. The particles were accelerated by a electrostatic dust accelerator to high speeds before they impacted polished aluminum targets. The projectile diameter and velocity ranged between 0.3 – 1.2 μm and 3 – 7 km/s, respectively. After bombardments, aluminum targets were analyzed by scanning electron microscopy to find craters and study their morphology. Based on the experiment results, the floors of impact craters created by iron projectiles are covered by projectile residues, and the shapes of the residues vary with impact velocities. On the contrary, there are no large residues visible from olivine projectile impacts. The ratio of crater diameter to particle diameter is similar for olivine and iron particles and it increases with impact velocity. This ratio is about 0.5 times smaller than for larger sized projectiles reported previously.

Key words: hypervelocity impact; micron-sized particle; crater morphology; olivine; iron.

1. INTRODUCTION

Micron-sized cosmic dust particles have attracted researchers' attention as they are a valuable resource for the fundamental data on small bodies in the universe, meanwhile, they also play as a messengers of their parent bodies. A micron-sized particle impacting onto a spacecraft at hypervelocity speed (usually defined as impact speed above 2 km/s) will leave mechanical damage and create impact products composed of a variety of gas molecules, ions, electrons and ejecta particles of different size. This happens frequently for micron-sized cosmic dust, as they are abundant in space. Common way to study the cosmic dust is the detection of impact effects like light flash[1], plasma[2, 3] and microphone[4] signals. Among the most simple is placing a smooth metallic or ductile material in space and retrieving it at a later date. The speed of the impact will depended on the relative speeds of the impactor and the target.

Analysis of the surface of the exposure material will then show small impact craters formed by the hypervelocity impacts. The resulting micron-sized craters can be investigated by optical or Scanning Electron Microscope (SEM) techniques[5, 6, 7]. The investigation of impact and penetration effects onto spacecraft surface materials has a long history. A number of spacecraft were used as collectors to study fluxes of cosmic dust and man-made grains in Low Earth Orbit (LEO). The most outstanding example is the Long Duration Exposure Facility (LDEF)[7]. The NASA Stardust spacecraft returned its sample capsule to Earth in 2006 [8], it not only visited comet Wild 2 in 2004, but also exposed its sample collector to the interstellar dust stream. Also the main part of Stardust dust collector aerogel, it also has approximately 100 cm^2 aluminum foil, which is practically analyzable. During its flyby of the comet, the encounter speed of the spacecraft is constrained as 6.1 km/s, which is easily achievable in the laboratory.

As comparisons, after these missions, many hypervelocity impact experiments have been carried out, establishing some damage equations and debris flux models. However, in reality, cosmic dust particles are micron-sized, irregular and brittle particles. Hence, there are still some uncertainties when we use these calibrations to infer properties of micron-sized cosmic dust from the craters on exposed collector samples.

In this study, we analyzed the morphology of the craters formed by 0.3 – 1.2 μm olivine and iron projectiles. These projectiles accelerated by a Van de Graaff accelerator, and impacted on polished aluminum surfaces at the velocity rangs from 3 km/s to 7 km/s.

Proc. '6th European Conference on Space Debris'
Darmstadt, Germany, 22–25 April 2013 (ESA SP-723, August 2013)

The goal was to obtain more detailed information on hypervelocity impact parameters from micron-sized silicate and metal projectiles. After bombardment of aluminum targets, scanning electron microscopy (SEM) was used to measure the diameters and depths of the impact craters.

2. DESCRIPTION OF EXPERIMENT FACILITIES

2.1. Accelerator

There are many different methods used for hypervelocity impact studies, like light gas guns, electromagnetic accelerators, and laser simulation. The Van de Graaff accelerators have become one of most suitable technologies for micron-sized particle acceleration, since the first report by Friichtenicht[9]. In a Van de Graaff accelerator, particles are charged and accelerated through a high voltage, becoming projectiles for impact experiments. The projectile velocity can be calculated using the following equation:

$$v = \sqrt{2QV/m} \tag{1}$$

where v is the velocity of the accelerated particle; Q is the particle charge; V is the potential of the accelerator and m is the particle mass. The Q/m value has an inverse relationship with particle radius, smaller particles could reach higher velocity after acceleration if other parameters are not changed. Moreover, larger velocities are obtained for particles of lower density materials.

Our experiments were carried out at the 2 MV Van de Graaff accelerator located at the Max Planck Institute for Nuclear Physics (MPIK, Heidelberg) and operated by IRS of the University of Stuttgart. The set-up of this accelerator is shown in Figure 1 and 2. After acceleration, charged projectiles travel along the beam tube, passing charge and velocity detectors, and then arrive at the particle selection unit (PSU) system[10]. When a suitable projectile arrives, the electrodes are grounded and let it pass through. The dust accelerator facility enables the acceleration of micrometer and submicron sized electrically conductive grains to speeds between 1 and 100 km/s. Single grains can be selected and their impact onto a target or experiment can be studied.

2.2. Projectiles–charged micron-sized particles

For the electrostatic acceleration to work, the particles must be capable of carrying surface charge and hence the range of materials used has been restricted to those which are either metal or those with a conductive coating. Table 1 shows the materials that have been used on the Van de Graff accelerator at MPIK.

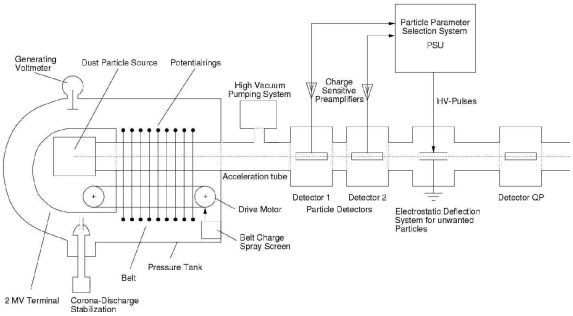

Figure 1. The sketch of a Van de Graaff with the particle selection unit (PSU) system.

Figure 2. The acceleration segment of the Van de Graaff accelerator at MPIK

Table 1. Accelerated dust materials [10]

Coating	Accelerated material	Size (μm)	Speed (km/s)
None	Iron	0.02-2.5	2-80
	Iron + Nickel	0.02-2.5	2-80
	Aluminum	0.1-4	1-50
	Carbon	0.2-1.4	1.5-26
	Carbon + Na	0.2-1.5	1.5-13
	Nickel	0.05-0.2	10-60
	Tungsten	0.1-4	1-40
	Tungsten carbide	0.1-4	1-40
	Cobalt	0.1-4	1-40
Zn, Au, Ag, Pt coated	SiO_2	0.1-5	1-30
	Pyroxene	0.05-4	0.5-35
	Anorthite	0.1-2.5	1-20
	Magnetite	0.05-0.44	4-24
	FeS	0.1-3	1-40
	Silica	0.1-3	1-40
PPy-Ps	Latex (1.6μm)	0.8-1.8	2-7.5
	Latex (0.4μm)	0.1-1.0	5-80
	Olivine	0.04-4	1-80
	Pyrrhotite	0.05-1.7	2-37
	Silica	0.2-2.5	2.5-15
PPy-PMPV	Latex(0.5μm)	0.5-1.5	7-30
PaNi-PS	Latex(0.75μm)	0.5-1.5	3.5-29

Olivine ($[Mg,Fe]_2SiO_4$) is a common mineral in meteorites and their parental asteroids, and well resembles siliceous cosmic dust with a hight melting point. However, due to olivine is a insulating materials, the particles have to be coated using the method described in detail by Hillier et al.[11]. Polypyrrole (PPy) coated olivine and iron particles were chosen as impactors for our experiments. Figure 3 shows the optical images of coated olivine particles. We decided to compare olivine shots with a well studied reference material of spherical shape for morphological analyzes. Spherical iron particles were considered as ideal in this respect, as they were used for a long time at the accelerator at MPIK (Figure 4). PPy coated olivine and iron grains have densities of 3.4 g/cm^3 and 7.8 g/cm^3, respectively. The sizes of olivine grains are nominal sizes, which are based on the assumption that all olivine grains are spheres.

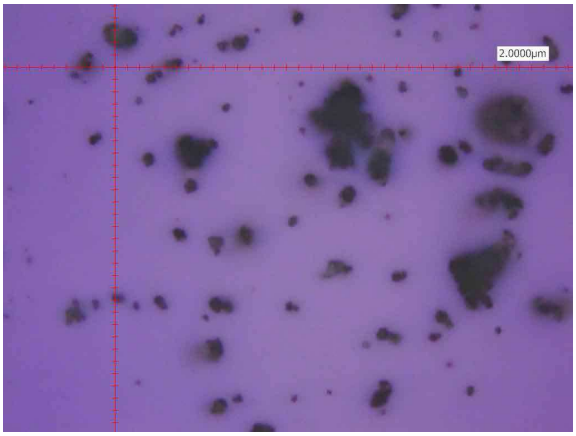

Figure 3. PPy-coated olivine grains optical image.

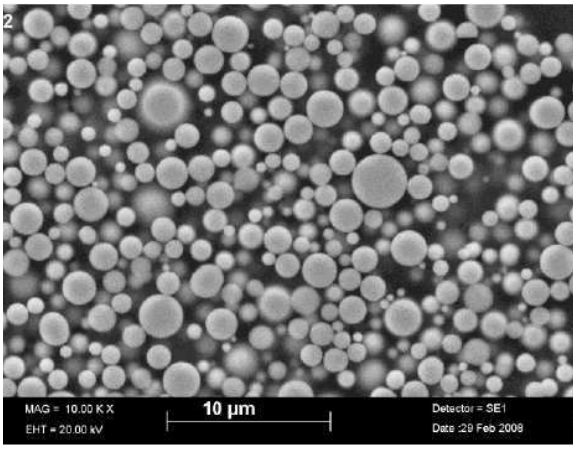

Figure 4. Iron particle grains SEM image[12].

Smaller particles could be accelerated to higher velocities. But for crater morphology studies, we need to choose suitable sizes and velocities for the projectiles to create observed craters. In our study, the sizes of olivine projectiles were chosen as 0.5 μm, 0.8 μm and 1.2 μm; and the velocities were 3 km/s, 5 km/s and 7 km/s, respectively. For iron projectiles the sizes were 0.3 μm, 0.4 μm, 0.5 μm, and 0.8 μm, and the velocities were 3 km/s, 4.5 km/s, 5 km/s and 7 km/s. The particles were chosen within a narrow window of diameter and velocity. The velocity was constrained to a range of 0.5 km/s around the selected velocity. The range of particles diameter is 0.1 μm around the selected size. For the largest olivine particles, their size range is expanded to 1.0 – 1.4 μm since the particle flux is extremely low in this case. The olivine and iron projectile selection windows are shown in Figure 5.

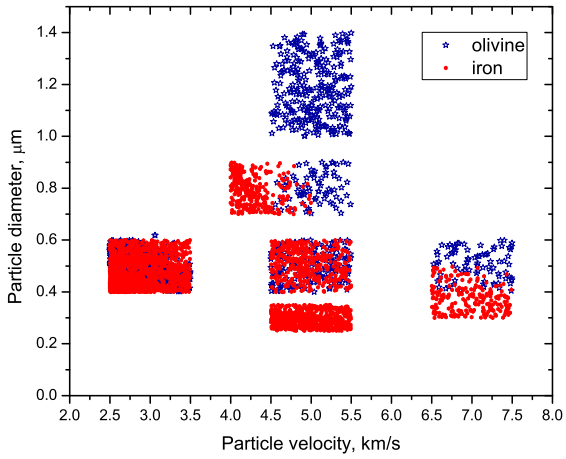

Figure 5. The range windows for selected particles.

2.3. Targets

Aluminum plates were chosen as impact targets. Their sizes were about 2 × 2 cm and the thicknesses were about 2 mm. In order to provide smooth surfaces, the targets were polished using routine procedures applied for mineralogical and geochemical thin section preparation. Figure 6 is an optical microscope image of a polished target surface. The hardness of these Al plates after polishing is about HB = 72 N/cm^2. To reduce differences in material parameters, each of the target surface was divided into five regions to test five different impact conditions for each projectile material. A 6 mm in diameter copper ring was used to limit particle impacts to the center area of each region. This procedure was also very helpful when we searched for impact craters.

3. DISCUSSION OF EXPERIMENTAL RESULTS

3.1. Crater imagines

After bombardment, the targets were examined by a scanning electron microscopy (SEM). SEM images of craters from individual olivine projectiles are shown in

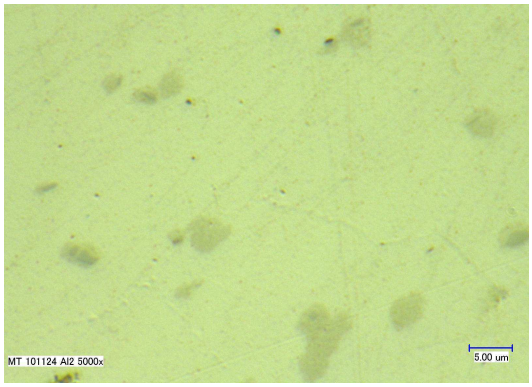

Figure 6. Image of a polished aluminum target by an optical microscope.

Figure 7. Figure 8 shows the morphology of craters created by iron projectiles. Unfortunately, we haven't found any craters in the size region 0.5 μm and 3 km/s for olivine projectiles.

In general, all crater shapes are nearly circular with a lip formed at the rim of the crater. Here, 'rim' is the complete circular confinement of the crater, the 'lip' is the irregular extension of the rim. However, there are some differences between olivine and iron projectiles. The rims of the craters created by olivine projectiles are not perfectly circular with not connected lips. This appears to be due to the effect of non-spherical shape of the projectiles. Iron projectiles created craters rims and lips that are circles and connected. Large residues from iron projectiles cover the craters' floors, and the shape of these residues varies with size and velocity of the projectiles. Most residues seem to be distributed over a larger area within the crater, either as ring (Figure. 8b,e) or area of a circle (Figure. 7c), however, the visibility is better for high impact velocities. In the case of olivine impact craters (Figure. 7), possibly tiny projectile residues can be identified in (Figure. 7a and 7c).

To determine the craters depths the angle between the SEM electron beam and the surface of the targets was varied from 90 degrees to 80 degrees by inclining the loading platform. According to a simple calculation the crater depth was obtained. All depths of craters created by olivine projectiles were measured. For iron projectiles, as there is a large sized residue covering on each crater floor in most case, it is almost not possible to get an accuracy value, only the depthes of the craters for 0.4 μm and 7 km/s projectiles were measured.

3.2. Discussion

The diameters (Dc) and depths (p) of all the measured craters are shown in Table 2. From the results, the ratio (R) of craters diameters (Dc) to projectiles diameters (Dp) depends on impact velocities. The average ratio R

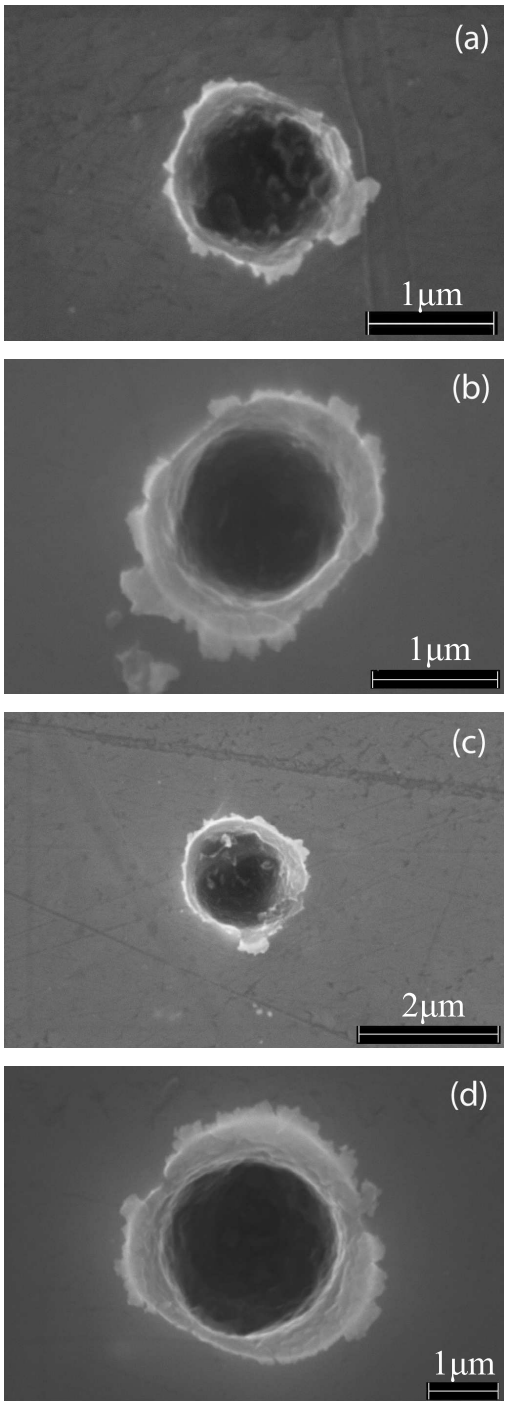

Figure 7. SEM images from olivine particles on aluminum target, impact parameters: (a)particle diameter is 0.5 μm, and particle velocity is 5km/s; (b)particle diameter is 0.5 μm, and particle velocity is 7 km/s; (c) particle diameter is 0.8 μm, and particle velocity is 5 km/s;(d) particle diameter is 1.2 μm, and particle velocity is 5 km/s. All the impacts are in normal angle.

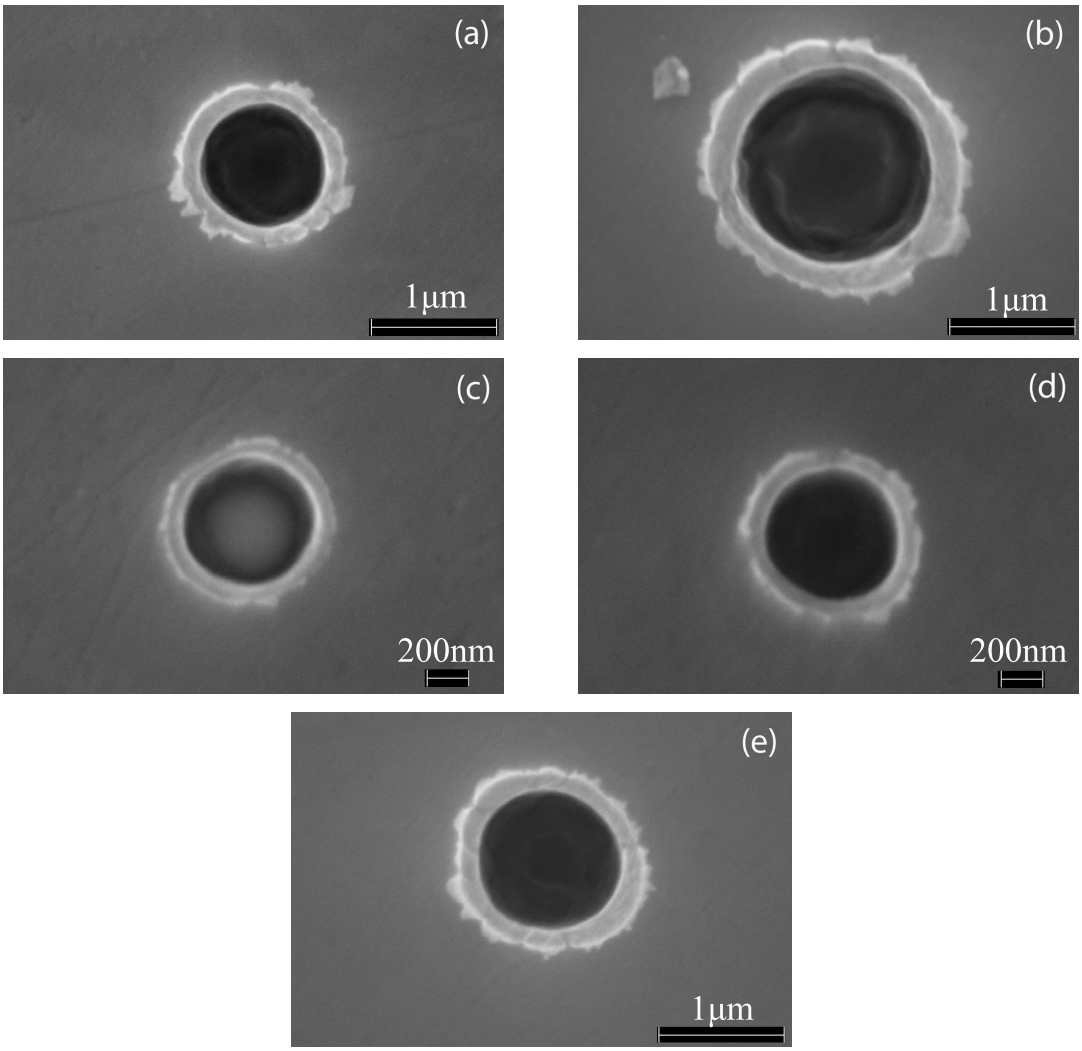

Figure 8. SEM images from iron particles on aluminum target, impact parameters: (a)particle diameter is 0.5 μm, and particle velocity is 5 km/s; (b)particle diameter is 0.8 μm, and particle velocity is 4.5 km/s; (c) particle diameter is 0.4 μm, and particle velocity is 7 km/s;(d) particle diameter is 0.5 μm, and particle velocity is 3 km/s;(e) particle diameter is 0.3 μm, and particle velocity is 5 km/s. All the impacts are in normal angle.

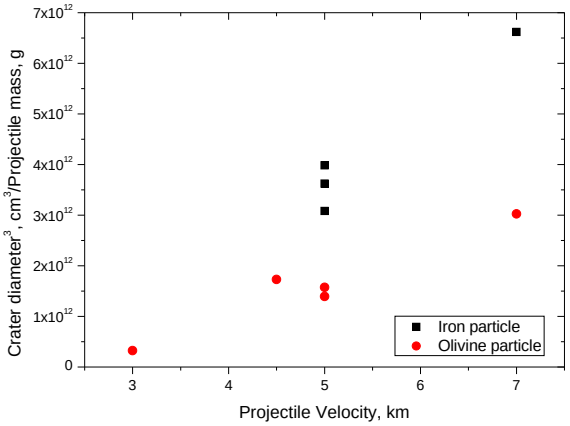

Figure 9. The relationship between impact velocity and crater diameter.

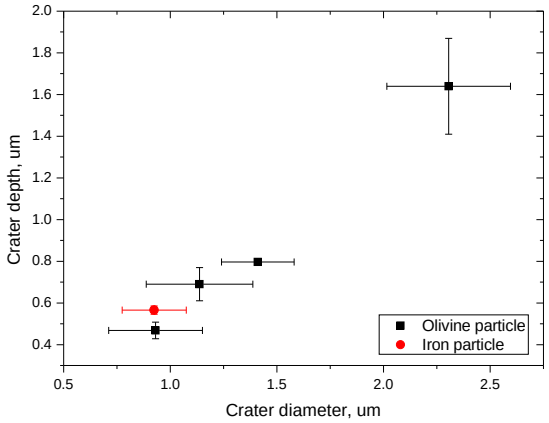

Figure 10. The relationship between craters diameter and crater depth(spherical).

are 1.84 and 2.28 for 5 km/s and 7 km/s olivine projectiles impacts. For iron projectiles, the values is 1.10, 1.85 and 2.32 for 3 km/s, 5 km/s and 7 km/s impacts, respectively. Comparing with the results from Kearsley et al.[13, 14], the ratio R is about 4.6, for 15 - 50 μm sized and 6.1 km/s soda-lime projectiles impacted onto 100 μm thick Al foil, which is about 2 times larger than our results. When considering the projectiles density, the relationship of projectiles mass, velocities and crater diameter is shown in Figure 9.

The ratio of craters diameters to craters depths (p) is about 1.65 for both iron and olivine projectiles. This value is a little larger than the value (Dc/p = 1) reported by Nagel et al.[15]. But for iron projectiles, further work is still needed, as most crater floors are covered by fragments.

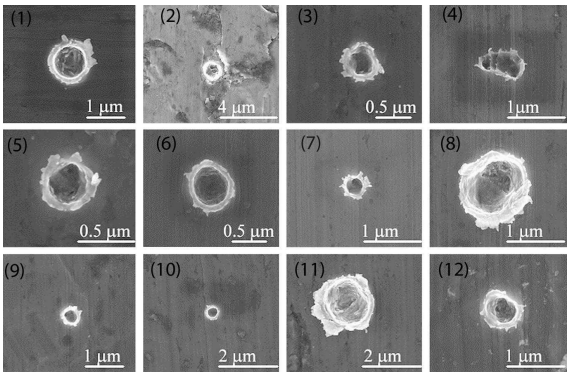

Figure 11. Micrographs of typical small impact features on stardust foil C100N [8].

3.3. Comparison with small crater population on Stardust aluminum targets

The NASA Stardust spacecraft flew through the coma of comet Wild 2 to capture cometary particles in low density silica Aerogel, and take the samples back to Earth. 100 μm thick aluminum foil between individual aerogel tiles served as holder. This foil also collected many craters with cometary particles [13, 14]. The micron-sized craters morphology in this aluminum foil is shown in Figure 11. Crater (1) shows a circular crater edge and the crater lip is a connected circle. This morphology resembles our experimental craters of spherical iron projectiles. Crater (6) has a connected lip but the crater rim is not circular: maybe it was created by a non-spherical cometary particle which had a smooth surface. The other craters resemble our experimental craters created by olivine projectiles.

4. CONCLUSIONS

We have performed impact catering experiments with micron-sized olivine and iron particles. Especially, olivine particle were used to simulate more realistic cosmic dust particles upon impact. The targets we chose were aluminum plates, as there are a number of space missions that exposed aluminum surfaces, which could be used for comparisons. There are some differences of crater morphologies resulting from olivine and iron projectiles. For iron projectiles the crater rims are circular and the crater lips are connected circles. When olivine projectiles impact on aluminum surfaces, the crater rims are not circular and the craters lips are not connected. These imperfect features are likely related to the non-spherical shapes and non-smooth surfaces of the olivine projectiles. There are some large residues covering the crater floors generated by iron projectiles. In contrast there are no large residues found on the crater floors of olivine projectiles. In agreement with former experiments, the value Dc/Dp of craters for micron-sized

Table 2. Summary of experimental and modeling results.

Material	Dia Dp (μm)	Velocity v (km/s)	Craters Measured	Crater Dia Dc	Crater Dep p (μm)	Dc/Dp (μm)	Dc/p
Olivine	0.5	5	7	0.93	0.47	1.86	1.97
	0.5	7	4	1.14	0.69	2.28	1.65
	0.8	5	6	1.41	0.80	1.76	1.76
	1.2	5	15	2.30	1.64	1.91	1.40
Iron	0.5	5	5	0.89	–	1.78	–
	0.8	4.5	8	1.53	–	1.91	–
	0.5	3	7	0.55	–	1.10	–
	0.3	5	5	0.56	–	1.87	–
	0.4	7	9	0.93	0.57	2.32	1.63

projectiles (0.3 - 1.2 μm) are about 0.5 times smaller than those of larger projectiles (15 - 50 μm).

ACKNOWLEDGEMENTS

The authors thank Dr. A. Varychev for his valuable assistance in SEM imaging of samples, and thank Dr. V. Sterken for discussion and language improvements.

REFERENCES

1. Eichhorn G., (1973). Measurements of the light flash produced by high velocity particle impact. *Planetary and Space Science*,**23**(11),1519–1525
2. Lee N., Close S., Lauben D., et al., (2012). Measurements of freely-expanding plasma from hypervelocity impacts. *International Journal of Impact Engineering*, **44**, 40–49
3. Srama R, Ahrens TJ, Altobelli N, et al., (2004). The Cassini Cosmic Dust Analyzer. *Space Science Reviews*, **114**(1-4), 465–518
4. Stradling G.L., Idzorek G.C., Keaton P.W., et al., (1990). Searching for momentum enhancement in hypervelocity impacts. *International Journal of Impact Engineering*, **10**(1–4), 555–570
5. Grün E., Horanyi M., Sternovsky Z., (2011). The lunar dust environment. *Planetary and Space Science*,**59**(14), 1672–1680
6. Hörz F., Brownlee D. E., Fechtig H., Hartung J. B., Et al., (1976). Lunar microcraters: Implications for the micrometeoroid complex. *Planetary and Space Science*,**23**(1), 151–172
7. Harvey G.A., (1991). Organic Contamination of LDEF, LDEF-69 Months in Space First Post-Retrieval Symposium. *NASA Conference Publication 3134 Part 1*, 179–196
8. Kearsley A. T., Borg J., Graham G. A., et al., (2008). Dust from comet Wild 2: Interpreting particle size, shape, structure, and composition from impact features on the Stardust aluminum foils. *Meteoritics and Planetary Science*, **43**(1-2), 41-73
9. Friichtenicht J. F., (1962). Two-million-Volt electrostatic accelerator for hypervelocity research. *Review of Scientific Instruments*,**33**(2), 209–212
10. Mocker A., Bugiel S., Auer S., et.al., (2011). A 2 MV Van de Graaff accelerator as a tool for planetary and impact physics research. Review of Scientific Instruments, **82**, 095111(1–8)
11. Hillier J.K., Sestak S., Green S.F., et al., (2009). The production of platinum-coated silicate nanoparticle aggregates for use in hypervelocity impact experiments. *Planetary and Space Science*, **57**, 2081–2086
12. Höfer C., (2010). Präparation und Analyse von Analogmaterial für extraterrestrischen Staub. *Bachelorarbeit vor Studiengang Geowissenschaften, Ruprecht-Karls-Universität Heidelberg*
13. Kearsley A. T., Graham G. A., Burchell M. J., et al., (2008). Micro-craters in aluminum foils: Implications of dust particles from comet Wild 2 NASA's Stardust spacecraft. *International Journal of Impact Engineering*, **35**, 1616–1624.
14. Leroux H., Borg J., Troadec D., et al., (2006). Microstructural study of micron-sized craters simulating Stardust impacts in aluminum 1100 targets. *Meteoritics and Planetary Science* **41**(2), 181–196
15. Nagel K., Fechtig H., (1980). Diameter to depth dependence of impact craters. *Planetary and Space Science*, **28**, 567–573